

Constant search time algorithm via topological quantum walks

D. O. Oriekhov,¹ Guliuxin Jin,¹ and Eliska Greplova¹

¹*Kavli Institute of Nanoscience, Delft University of Technology, 2628 CJ Delft, the Netherlands*
(Dated: June 28, 2024)

It is well-known that quantum algorithms such as Grover's can provide a quadratic speed-up for unstructured search problems. By adding topological structure to a search problem, we show that it is possible to achieve a constant search-time quantum algorithm with a constant improvement of the search probability over classical search. Specifically, we study the spatial search algorithm implemented by a two-dimensional split-step quantum random walks that realize topologically non-trivial phases and show the asymptotic search behavior is constant with growing system size. Using analytical and numerical calculations, we determine the efficient search regions in the parameter space of the quantum walker. These regions correspond to pairs of trapped states formed near a lattice defect. By studying the spectral properties of the discrete time-evolution-operators, we show that these trapped states have large overlap with the initial state. This correspondence, which is analogous to localization by constructive interference of bound states, makes it possible to reach the best possible search-time asymptotic and produce a disorder-protected fast search in quantum random walks.

Quantum search algorithm, Grover's search [1], is known as an algorithm that demonstrates quantum advantage over its classical analogue. Grover's algorithm performs a search of marked element in an unstructured database with a given probability with asymptotic time being a square root of database element count. However, its implementation depends on an oracle operator - a way of distinguishing marking element that applies to a whole quantum state. The quantum random walks are known as an example of natural implementation of such an oracle operator [2–6]. The discrete-time quantum random walks are defined as a set of shift and spin flip operators applied at the whole system at each time step. The successful search event is defined as a time of maximum localization of quantum walker on a defect when starting from a uniform distribution over all system.

Although, different kinds of quantum walks demonstrate a Grover-type convergence of a spatial search in two and higher dimensions, the dependence on spin flip operator and position of defect site relative to remaining system is crucial and in many cases results in a decreased efficiency of search algorithm [4, 5, 7]. The latter fact also serves as a motivation for the search for sub-optimal yet more robust to disorder and element positioning algorithms, that would provide quantum advantage. In the present paper we study the two-dimensional split-step quantum random walks that are analogues of Chern topological insulators [8] in crystalline solids. The similar split-step QRW in 1D were studied in Refs.[9, 10] and a number of our conclusions made below might work also in those cases. By analyzing the parameter spaces of quantum walker and defect, we find that there exist sets of parameters that demonstrate efficient search of a given defect (see a search probability map in Fig.1). Below we show that these regions in parameter space can be categorized into two distinct classes based on their position inside the topological phase or on the phase separation

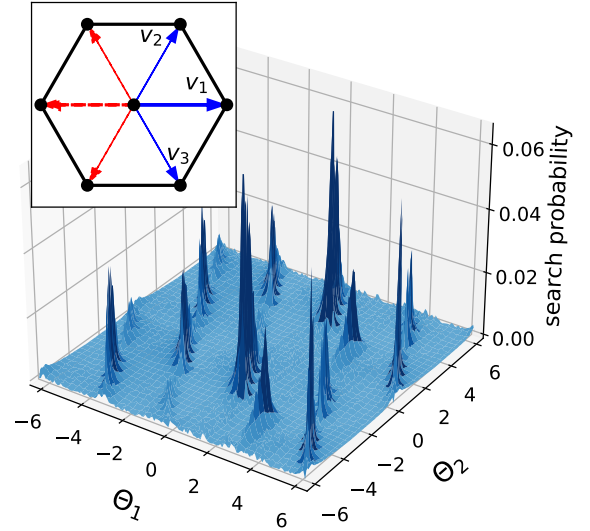


FIG. 1. The success probability of search algorithm as a function of QRW parameters $\Theta_{1,2}$ (see Eq.(2)) for a defect with $\Theta_1^{def} = 5\pi/8$, $\Theta_2^{def} = \pi/2$. High peaks are of order of magnitude larger than average localization probability and correspond to parameters for which quantum walker performs search efficiently. Inset: geometry of split-step QRW on a triangular lattice with three shift vectors \mathbf{v}_i - solid ones correspond to shift of spin up components, dashed $-\mathbf{v}_i$ for spin down.

lines. Notably, the search time for the parameters inside both classes of regions demonstrates saturation to a constant search time with growing system size. The saturation of search time happens at different system sizes, while before that the square root time growth behavior takes place.

The constant search time asymptotic was previously identified only for electric Dirac QRW with non-local marking of defect in the form of Coulomb potential

[11, 12]. The non-locality creates an important difference from our algorithm. Namely, here the constant search time is achieved with local marking, thus making it directly implementable in experimental memory setup.

Below we analyze in detail the time evolution of states for a range of quantum walker parameters and study the overlap of initial state with the eigenstates of a unitary operator corresponding to a single time step of QRW. We demonstrate that the search speedup with constant time asymptotic is related to the appearance of trapped states of a specific structure near the defect: the two pairs of trapped states should simultaneously have a large matrix element of coordinate operator of the defect and the large overlap with initial uniformly distributed state. In the mathematical sense the trapped states are defined as a states that have compact support and zero density elsewhere. Their analogue in quantum mechanics are the strongly localized bound states on impurity in a system. We note that a number of mathematically rigorous studies have been made for spectral properties of quantum random walks and trapped states [5, 9, 13–16] together with their dynamics [17, 18]. However, the possible efficiency of search algorithm based on exploiting the particular structure of QRW was not previously addressed. The strong dependence of the trapped states structure on defect and walker parameters also suggests a scenario of protecting quantum search from a random disorder by an appropriate fine-tuning of marking parameters for the searched element.

The quantum random walk deployed for algorithmic speed-up in this work was firstly introduced in Ref.[8] as a way to simulate topological insulators. Its single time step

$$\Psi(t+1) = U(\Theta_1, \Theta_2)\Psi(t) \quad (1)$$

is defined via three rotations of spin and subsequent translations:

$$U(\Theta_1, \Theta_2) = T_{v_3} R(\theta_1) T_{v_2} R(\theta_2) T_{v_3} R(\theta_1), \quad (2)$$

$$R(\theta) = \begin{bmatrix} \cos(\theta/2) & -\sin(\theta/2) \\ \sin(\theta/2) & \cos(\theta/2) \end{bmatrix}.$$

The translation operations shift spin up components by $+\mathbf{v}_i$ and spin down by $-\mathbf{v}_i$. The vectors $\mathbf{v}_{1,2,3}$ can be defined on a triangular lattice as $\mathbf{v}_1 = (1, 0)$, $\mathbf{v}_2 = (1/2, \sqrt{3}/2)$ and $\mathbf{v}_3 = (1/2, -\sqrt{3}/2)$, see inset in Fig.1.

The spectrum of quasi-energies of this QRW without defects has two particle-hole symmetric bands due to matrix $U(\Theta_{1,2})$ being real. The corresponding states of $\pm E$ energy are related by complex conjugation $\Psi^{-E} = (\Psi^E)^*$. Depending on parameters $\Theta_{1,2}$, such QRW realizes distinct topological phases with Chern numbers of Floquet-type bands $C = \pm 1, 0$. To make a contrast with same kind of topological insulators [19, 20] in crystalline solids, we note that QRW spectrum is defined as Floquet-type quasi-energies, thus being limited to $(-\pi, \pi)$ interval. The gap closing happens either at zero energy or at

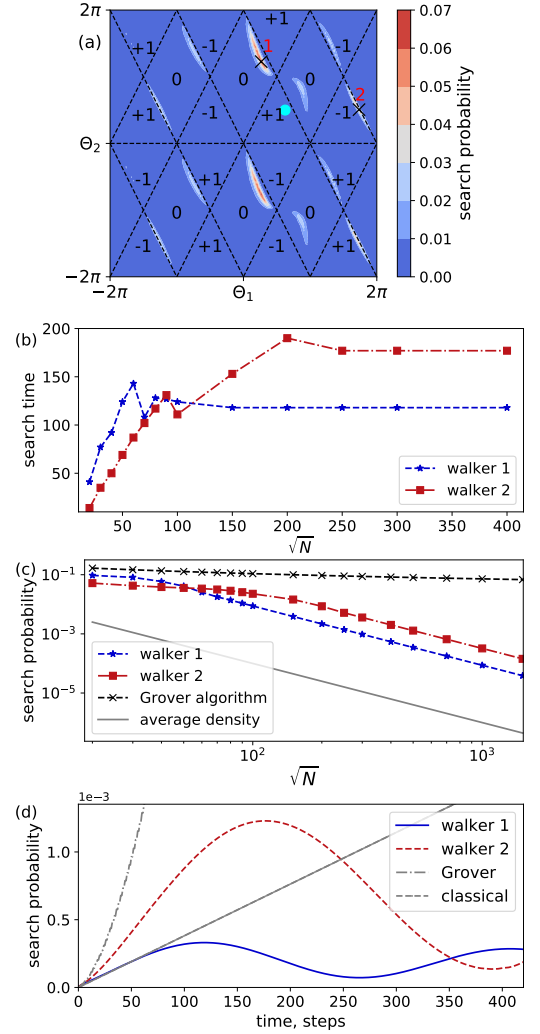


FIG. 2. (a) A colormap representation of a maximum localization probability on a defect site over the evolution time $T = 1000$ for a system of size $N = 40 \times 40$ starting from a fully uniform distribution. Black numbers indicate Chern numbers of the corresponding parameter regions and dashed lines correspond to phase separation lines. Cyan dot marks the defect parameters $(5\pi/8, \pi/2)$. (b) Search time measured as a position of first probability peak as a function of system size for walker parameters indicated by crosses ‘1’ and ‘2’ in panel (a). (c) Search probability dependence on system size. The two regions of different dependence are present where probability follows Grover-type scaling $P \sim 1/\log(N)$ until the time asymptotic changes to constant in (b) and then switches to system size scaling $P \sim 1/N$ but having few orders of magnitude larger value than average density in the system. (d) Comparison of performance with Grover’s algorithm and repeated classical search for system size $\sqrt{N} = 512$. Walker 2 shows advantage over classical.

the ends of interval on the phase separation lines indicated in Fig.2(a), and at $\Theta_2 = 0$ line - gap closes everywhere [21].

In our setup the search algorithm goal is defined as a

problem of finding a single node on a finite 2D lattice of size $\sqrt{N} \times \sqrt{N}$ unit cells starting from initial state $|i\rangle$. We apply the periodic boundary condition in order to avoid the appearance of edge states. The searched node is marked by parameters $\Theta_{1,2}^{def}$ that are different from surrounding $\Theta_{1,2}$. To estimate the possibility of given quantum walker to perform search efficiently, we firstly scan the entire parameter range $\Theta_{1,2}$ for a given defect values $\Theta_{1,2}^{def}$. The performance of search algorithm is measured by a search probability. It is defined as a peak $\max_{t \in [0, T]} P_{def}(t)$ in time-dependent density of the system state at the defect node,

$$P_{def}(t) = |\langle d | \Psi(t) \rangle|^2, \quad (3)$$

where $|d\rangle = \sum_{\sigma=\uparrow, \downarrow} |x = def, \sigma\rangle$ is the defect coordinate operator with both components of spin σ , and $|i\rangle$ is the initial state of the system defined as $|i\rangle = \frac{1}{\sqrt{2N}} \sum_{\sigma, x} |x, \sigma\rangle$ with summation over entire system. The plot of the maximum value of density $P_{def}(t)$ on defect over the interval of time $T = 1000$ for test system size $N = 40 \times 40$ sites is shown in Fig.1 for $\Theta_{1,2}^{def} = (5\pi/8, \pi/2)$. In Fig.2(a) we show the colormap representation of the same search probability distribution on the top of phase diagram in parameter space (see also Supplement [21] for other defect parameters).

The islands of efficient search in parameter space fill a small areas placed in two distinct types of regions: inside topological phases and on phase separation lines. We compare the search time and probability behavior with growing system size for the walker parameters marked by ‘1’ and ‘2’ in the Fig.2(a), that realize best search probability within its regions. Such results are shown in Fig.2(b). With the growing system size the behavior of search time defined via first probability peak demonstrates qualitative change - from $T \sim \sqrt{N}$ dependence to $T \sim const$ in both curves. As we noted previously, such speed-up was observed only for the Dirac QRW with particular type of Coulomb-like disorder potential [11, 12]. In Fig.2(c) the search probability dependence of walkers ‘1’ and ‘2’ on system size is compared with average density at non-defect nodes and Grover’s algorithm search probability. We find that the constant search time regime corresponds to the $P_{def}(t) = O(1/N)$ with a large numerical prefactor. This decrease of search probability with system size N is faster than Grover’s one, $P_{def}^{Grover} = O(1/\log N)$. The search probability dependence in the form $O(1/N)$ arises due to the trapped states having finite support. The system size grows beyond the trapped state support size corresponds to saturation of search time asymptotic to constant and clear change in probability dependence curve in Fig.2(c). To check the dependence of search probability on defect parameters for given walker we performed the same 2D parameter space calculation taking walker “1” and checking $\Theta_{1,2}^{def} \in [-2\pi, 2\pi]$. It is found that the search probability

does not depend on Θ_2^{def} [21], thus the more informative is to present a dependence on Θ_1^{def} as shown in Fig.3(a).

The asymptotic scaling of $O(1/N)$ in search probability does not reach the optimal Grover scaling, but still provides constant improvement over the classical search algorithm. The probability of classical algorithm grows as t/N with multiple trials, t (one per time step). For this purpose, in Fig.2(d) we present a comparison of probability on searched node as a function of time for two walkers marked in Fig.2(a), Grover’s search for split-step QRW from Ref.[7] and a classical search. The walker ‘2’ demonstrates twice as large probability as classical search, while the walker ‘1’ follows the classical search probability for approximately 100 steps. In terms of detection via measurements, higher probability on a node means that the detector resolution used to identify position could be lower - in particular, for walker ‘1’ the detection resolution could be 100 times smaller than for classical probes of individual nodes. The Grover’s algorithm performance demonstrates even higher probability at the same time scale, which makes it advantageous in the non-disordered system. As we point out below, that advantage of Grover’s search might be lost in a disordered systems.

To describe the origin of different speed-ups in this system and why the regions of efficient search represent a small fraction of parameter space, we analyze the spectrum and localization properties of eigenvectors of a unitary operator of system with one defect. The probability evolution at a defect site at discrete times t can be rewritten through the unitary operator of QRW,

$$P_{def}(t) = |\langle d | \bar{U}^t(\Theta_1, \Theta_2) | i \rangle|^2. \quad (4)$$

The \bar{U} notation is introduced in order to underline that unitary operator takes into account defect site. Substituting the eigenbasis decomposition of the \bar{U} operator, $\bar{U}|n, \pm\rangle = e^{i\pm E_n} |n, \pm\rangle$, we have

$$P_{def}(t) = \left| \langle d | \sum_{n, \lambda=\pm} e^{i\lambda E_n t} |n, \lambda\rangle \langle n, \lambda | i \rangle \right|^2 \quad (5)$$

The saturation of search time to constant scaling after system size becomes large enough suggests that the properties of states that mainly contribute to the Eq.(5) do not change with system size. This feature directly corresponds to the definition of trapped states previously introduced in Refs. [5, 13] in the context of QRWs staying localized around its initial starting node over infinite evolution time. We investigate the contribution of different eigenstates of \bar{U} to the evolution of probability, $P(t)$, in Fig.3(b) by comparing the product of overlaps $|\langle d | n, \lambda \rangle \langle n, \lambda | i \rangle|^2$. The panels in Fig.3(b) correspond to different parameters of defect denoted by vertical dashed lines for walker ‘1’ in Fig.3(a).

The scale of x -axis in each panel of Fig.3(b) shows that defect parameters with higher search probability also cor-

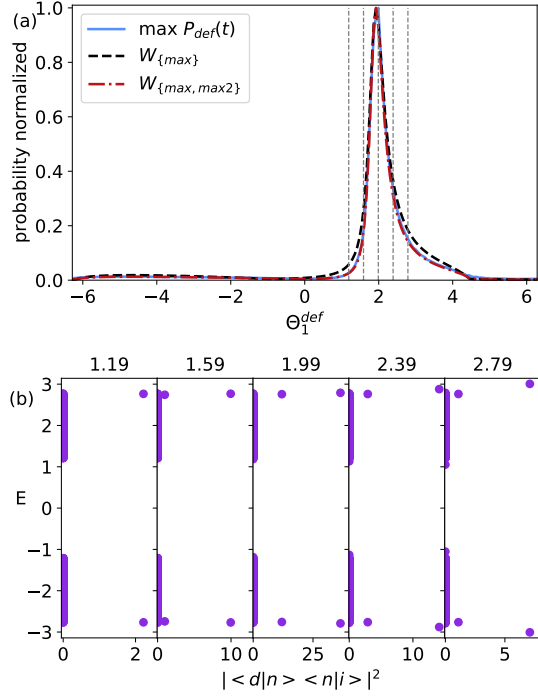


FIG. 3. (a) Comparison of maximum value of probability on defect for a walker ‘1’ from Fig.2 as a function of defect parameter Θ_1^{def} with the maximal value of squared of overlaps defined in Eq.(6) with \mathcal{M} containing one and two states respectively. All quantities are normalized to scale (0,1) for the purpose of comparison. The summation over two trapped states gives very accurate approximation of search probability peak. (b) The squared product of overlaps plotted as a function of energy of each eigenstate of operator \bar{U} for walker parameter ‘1’ and defect parameter Θ_1 indicated on top of each panel. Trapped states differ from other states by significantly higher value of overlap.

respond to higher overlap product for a few states - in this case two pairs of particle-hole symmetric states. To further verify this observation, we compare the maximal value of overlap product

$$W_{\mathcal{M}} = \left| \sum_{n \in \mathcal{M}, \lambda = \partial} \langle d | n, \lambda \rangle \langle n, \lambda | i \rangle \right|^2 \quad (6)$$

of a single eigenstate of \bar{U} with the normalized probability dependence $\max[P_{def}(t)]$ as function of Θ_1^{def} . The comparison is made by taking a single pair of states that maximize overlap with set of indices $\mathcal{M} = \{n_{max}\}$, as well as two pairs of states $\mathcal{M} = \{n_{max}, n_{second\ max}\}$. The results presented in Fig.3(a) indicate that while $\mathcal{M} = \{n_{max}\}$ selection overestimates the region of good search, the $\mathcal{M} = \{n_{max}, n_{second\ max}\}$ very precisely describes the high search probability peak. To further check this correspondence between the evolution of described by two pairs of states with maximal overlap and the max probability distribution, we plotted the same comparison for a defect $\Theta_{1,2}^{def} = (5\pi/8, \pi/2)$ along phase separation line

and the line with walker ‘1’ in Supplemental material. The correspondence for a test system size with $\sqrt{N} = 40$ shows that efficient search for such split-step QRW is mostly determined by the appearance of two pairs of trapped states having large overlap with both defect and initial state.

Finally, we perform a comparison of time evolution defined by two pairs of trapped states that maximize overlap criteria with the evolution of probability on the defect. For this purpose we note that the \bar{U} has the same particle-hole symmetry as $U(\Theta_{1,2})$ because it is a real matrix. In addition, by calculating overlap products denoted as $w_{\pm,j}^{\sigma} = \langle d, \sigma | j \rangle \langle j | i \rangle$ for each spin $\sigma = \uparrow, \downarrow$ and pair of trapped states j at the defect site separately, we find that for each trapped state there is a phase difference $w_{+,j}^{\downarrow} = iw_{+,j}^{\uparrow}$ and corresponding $w_{-,j}^{\downarrow} = -iw_{-,j}^{\uparrow}$ up to numerical precision. The former symmetry is present only at defect site and is a property of trapped states localized around the defect. Thus, evolution of both spin components at the defect site that is generated by trapped states is described as follows

$$\Psi_{\uparrow,d}(t) = 2 \sum_{j=1,2} |w_{+,j}^{\uparrow}| \cos(E_j t + \arg(w_{+,j}^{\uparrow})), \quad (7)$$

$$\Psi_{\downarrow,d}(t) = 2 \sum_{j=1,2} |w_{+,j}^{\uparrow}| \sin(E_j t + \arg(w_{+,j}^{\uparrow})), \quad (8)$$

where we took into account the particle-hole symmetry relation $w_{-,j}^{\sigma} = (w_{+,j}^{\sigma})^*$. It is important to emphasise that after calculating probability at a defect site, one finds that the two spin components exactly cancel oscillating parts of each other for a single value of j due to the different phase of oscillations between \sin and \cos in equations (7),(8) above

$$|\Psi_{\sigma,d}^j(t)|^2 = 2 |w_{+,j}^{\uparrow}|^2 \times \left(1 + \text{sign}(\sigma) \cos(2E_j t + 2\arg(w_{+,j}^{\uparrow})) \right), \quad (9)$$

with $\text{sign}(\sigma) = \pm$. Thus, the contribution of each single pair of trapped states is constant and due to the initial condition of uniformly distributed state over entire system it could not describe the peak in probability. However, the crucial contribution comes from the superposition between two pairs of trapped states and is manifested in the last oscillating term in the total density evolution at the defect:

$$|\Psi_{\uparrow,d}(t)|^2 + |\Psi_{\downarrow,d}(t)|^2 = 4 \left(|w_{+,1}^{\uparrow}|^2 + |w_{+,2}^{\uparrow}|^2 \right) + 8 \times |w_{+,1}^{\uparrow}| |w_{+,2}^{\uparrow}| \cos((E_1 - E_2)t + \arg w_{+,1}^{\uparrow} - \arg w_{+,2}^{\uparrow}). \quad (10)$$

The period of this oscillation is different from the fast oscillations of each trapped states and defined by the energy difference between the positive energy levels of two

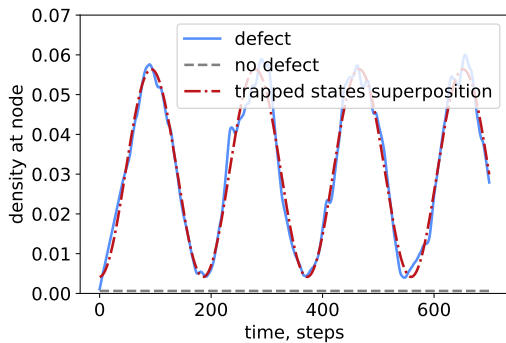


FIG. 4. The comparison of density evolution at searched defect node (blue solid line) and another distanced node without defect (gray dashed line) with time for a walker parameters ‘1’ and defect marked by $(5\pi/8, \pi/2)$. The red dash-dotted line corresponds to the evolution described by only two pairs of trapped states that maximize product of overlaps and given by Eq.(10). The evolution from trapped states approximates with very good precision the first few peaks in probability and the time of their occurrence.

pairs of trapped states ($E_1 - E_2$). The plot of evolution of probability on defect in Fig.4 shows that such simple expression captures very well the structure of oscillations, the time of first peak appearance and the max probability on the first period on a defect. In Fig.4 the results are presented for a walker ‘1’, and the same is shown for a walker ‘2’ in Supplemental material. Another way to check the agreement of predicted period of oscillations with the actual oscillation of probability on a defect node we used numerical Fourier transform. The agreement with period defined by $(E_1 - E_2)$ has errors below 2% on the timescale of evolution $T = 5000$ for system with $\sqrt{N} = 40$ [22]. Note that such definition of period through the difference of eigenstates of operator is different from the common one used in Grover’s search in QRW [7, 23]. Specifically, the period definition we use here is between states from different particle-hole symmetric pairs rather than between states from single pair.

The change of time asymptotic that is shown in Fig.2(b) happens when the system size becomes larger than diameters of both trapped state pairs. In Supplemental material [21] we show that the state from the pair with smaller overlap in Fig.2(c) has larger radius of localization (95% of the probability density). This pair of states determines the chance in the search time asymptotic as shown in Fig. 2b.

Finally, we note on stability of algorithm in comparison with Grover’s search. In Supplemental material [21] we present a comparison from Fig.2(d) for the disordered systems with disorder being implemented in rotation angles. In the large disorder cases walker ‘2’ shows similar or even better performance than Grover’s search imple-

mented via QRW, and is also advantageous against classical search.

In conclusion, we demonstrated that a fast quantum search algorithm can be realized in topological split-step quantum random walks. We proposed a concrete implementation of this search consisting of the following steps, namely (i) Check the appearance of pair of trapped states near a defect and overlap product maximization criteria for a small system; (ii) apply the same encoding of searched site in the large system with the same walker parameters; (iii) initialize uniform state in the large system; (iv) the high density peak in time will reveal the searched node position [24]. Our algorithm admittedly relies on the proper tuning of walker and searched node parameters. At the same time this property also allows for a protection against disorder with Θ_1 parameter values being not within efficient search interval. Interestingly, in the search algorithm we present here the ‘structure’ is induced in a quantum way (via dynamically appearing interference pattern due to overlap with trapped states) after fixed amount of time, i.e. it is not known a-priori where the pairs of trapped states are localized. In such formulation, our algorithm is suitable to make fast detectors of emergent defects in topological split-step quantum random walks. In addition, we point out that the dependence of algorithm of superposition of only four states makes it less sensitive to disorder rather than Grover’s algorithm, which performs optimally when a significant percentage of states contributed into constructive interference. Our search algorithm, as formulated in this work, can be immediately tested in photonic and synthetic lattice quantum walk experiments that realize topological QRW [25–28].

Acknowledgements. We benefited from discussions with Anton Akhmerov, Yaroslav Herasymenko, Margarita Davydova and Carlo Beenakker. This project was supported by the Kavli Foundation. This publication is part of the project Engineered Topological Quantum Networks (with Project No. VI.Veni.212.278) of the research program NWO Talent Programme Veni Science domain 2021 which is financed by the Dutch Research Council (NWO). G.J acknowledges the research program “Materials for the Quantum Age” (QuMat) for financial support. This program (registration number 024.005.006) is part of the Gravitation program financed by the Dutch Ministry of Education, Culture and Science (OCW).

-
- [1] L. K. Grover, A fast quantum mechanical algorithm for database search, in *Proceedings of the Twenty-Eighth Annual ACM Symposium on Theory of Computing* (ACM Press, Philadelphia, PA, 1996) p. 212–219.
 - [2] N. Shenvi, J. Kempe, and K. B. Whaley, Quantum random-walk search algorithm, *Physical Review A* **67**, 052307 (2003).

- [3] A. M. Childs and J. Goldstone, Spatial search by quantum walk, *Physical Review A* **70**, 022314 (2004).
- [4] A. Ambainis, J. Kempe, and A. Rivosh, Coins make quantum walks faster, *Proc. 16th ACM-SIAM SODA* **16**, 1099 (2005), [arXiv:quant-ph/0402107 \[quant-ph\]](#).
- [5] N. Inui, Y. Konishi, and N. Konno, Localization of two-dimensional quantum walks, *Physical Review A* **69**, 052323 (2004).
- [6] D. Reitzner, M. Hillery, E. Feldman, and V. Bužek, Quantum searches on highly symmetric graphs, *Physical Review A* **79**, 012323 (2009).
- [7] M. Roget, H. Kadri, and G. D. Molfetta, Optimality conditions for spatial search with multiple marked vertices, *Physical Review Research* **5**, 033021 (2023).
- [8] T. Kitagawa, M. S. Rudner, E. Berg, and E. Demler, Exploring topological phases with quantum walks, *Physical Review A* **82**, 033429 (2010).
- [9] T. Endo, H. Kawai, and N. Konno, The stationary measure for diagonal quantum walk with one defect, *Interdisciplinary Information Sciences* **23**, 57 (2017).
- [10] T. Endo, N. Konno, and H. Obuse, Relation between two-phase quantum walks and the topological invariant, *Yokohama Mathematical Journal* , 66 (2021), [arXiv:1511.04230 \[math-ph\]](#).
- [11] J. Zylberman and F. Debbasch, Dirac spatial search with electric fields, *Entropy* **23**, 1441 (2021).
- [12] T. Fredon, J. Zylberman, P. Arnault, and F. Debbasch, Quantum spatial search with electric potential: Long-time dynamics and robustness to noise, *Entropy* **24**, 1778 (2022).
- [13] N. Inui, N. Konno, and E. Segawa, One-dimensional three-state quantum walk, *Physical Review E* **72**, 056112 (2005).
- [14] T. Fuda, A. Narimatsu, K. Saito, and A. Suzuki, Spectral analysis for a multi-dimensional split-step quantum walk with a defect, *Quantum Studies: Mathematics and Foundations* **9**, 93 (2021).
- [15] M. Maeda, Asymptotic stability of small bound state of nonlinear quantum walks, *Physica D: Nonlinear Phenomena* **439**, 133408 (2022).
- [16] T. Fuda, D. Funakawa, S. Sasayama, and A. Suzuki, Eigenvalues and threshold resonances of a two-dimensional split-step quantum walk with strong shift, *Quantum Studies: Mathematics and Foundations* **10**, 483 (2023).
- [17] T. Fuda, D. Funakawa, and A. Suzuki, Localization of a multi-dimensional quantum walk with one defect, *Quantum Information Processing* **16**, 10.1007/s11128-017-1653-4 (2017).
- [18] J. Mares, J. Novotný, M. Štefáňák, and I. Jex, Key graph properties affecting transport efficiency of flip-flop Grover percolated quantum walks, *Physical Review A* **105**, 062417 (2022).
- [19] A. Kitaev, V. Lebedev, and M. Feigel'man, Periodic table for topological insulators and superconductors, in *AIP Conference Proceedings* (AIP, 2009).
- [20] F. D. M. Haldane, Model for a quantum Hall effect without Landau levels: Condensed-matter realization of the “parity anomaly”, *Physical Review Letters* **61**, 2015 (1988).
- [21] (), see Supplemental Material at [] for the visualization of localization probability distribution for different defect parameters, more detailed numerical comparison of spectral properties with time asymptotics, and the performance of search algorithms in disordered systems.
- [22] (), the code for all simulations performed in the paper can be found at the following zenodo: doi: 10.5281/zenodo.12554735 and gitlab: <https://gitlab.com/QMAI/papers/topologicalsearch> repositories.
- [23] T. G. Wong, Corrigendum: Grover search with lackadaisical quantum walks (2015 j. phys. a: Math. theor. 48 435304), *Journal of Physics A: Mathematical and Theoretical* **51**, 069501 (2018).
- [24] In our case the possibility of dark states influencing the quality of the search is not considered as they are not found in the simulated systems and are not expected to appear near single node defect. The dark states are degenerate trapped states that are orthogonal to detector state. [29, 30].
- [25] T. Kitagawa, M. A. Broome, A. Fedrizzi, M. S. Rudner, E. Berg, I. Kassal, A. Aspuru-Guzik, E. Demler, and A. G. White, Observation of topologically protected bound states in photonic quantum walks, *Nature Communications* **3**, 882 (2012).
- [26] C. Chen, X. Ding, J. Qin, Y. He, Y.-H. Luo, M.-C. Chen, C. Liu, X.-L. Wang, W.-J. Zhang, H. Li, L.-X. You, Z. Wang, D.-W. Wang, B. C. Sanders, C.-Y. Lu, and J.-W. Pan, Observation of topologically protected edge states in a photonic two-dimensional quantum walk, *Physical Review Letters* **121**, 100502 (2018).
- [27] T. Nitsche, T. Geib, C. Stahl, L. Lorz, C. Cedzich, S. Barkhofen, R. F. Werner, and C. Silberhorn, Eigenvalue measurement of topologically protected edge states in split-step quantum walks, *New Journal of Physics* **21**, 043031 (2019).
- [28] C. Esposito, M. R. Barros, A. Durán Hernández, G. Carvacho, F. Di Colandrea, R. Barboza, F. Cardano, N. Spagnolo, L. Marrucci, and F. Sciarrino, Quantum walks of two correlated photons in a 2D synthetic lattice, *npj Quantum Information* **8**, 34 (2022).
- [29] F. Thiel, I. Muelem, D. Meidan, E. Barkai, and D. A. Kessler, Dark states of quantum search cause imperfect detection, *Physical Review Research* **2**, 043107 (2020).
- [30] F. Thiel, I. Muelem, D. A. Kessler, and E. Barkai, Uncertainty and symmetry bounds for the quantum total detection probability, *Physical Review Research* **2**, 023392 (2020).

Supplemental material for “Constant search time algorithm via topological quantum walks”

by D. O. Oriekhov, Guliuxin Jin, and Eliska Greplova

CONTENTS

References	5
Properties of split-step quantum random walk	1
The comparison of product of overlaps with optimal search regions	2
Structure of trapped states in coordinate space	3
Stability of search algorithm with disorder	3

Properties of split-step quantum random walk

In this section we present a number of properties for split-step QRW that realizes topological phases in the case without defect nodes. Using Eq.(1) from the main text, and assuming the infinite system in both directions, we find the following equation for spectrum of translation-invariant unit cell:

$$\lambda^2 + 2\lambda \cos(\Theta_2/2) (\sin^2(\Theta_1/2) \cos(2k_y) - \cos^2(\Theta_1/2) \cos(k_x)) + \lambda \sin(\Theta_1) \sin(\Theta_2/2) (\cos(k_x - 2k_y) + 1) + 1 = 0. \quad (S1)$$

The solution of this equation, $\lambda_{\pm} = e^{iE}$, gives a particle-hole symmetric spectrum of quasi-energies. The quasi-energy is given by

$$E = \pm \arccos \frac{b}{\sqrt{2b^2 - 4}},$$

$$b = 2 \cos(\Theta_2/2) (\sin^2(\Theta_1/2) \cos(2k_y) - \cos^2(\Theta_1/2) \cos(k_x)) + \sin(\Theta_1) \sin(\Theta_2/2) (\cos(k_x - 2k_y) + 1) \quad (S2)$$

The topological phases and corresponding Chern numbers were defined in Ref.[8]. The phase separation lines are characterized by the gap closing. For the technical purposed of identifying different types of search speed up discussed in the main text, we plot a map of gap value: the minimal gap value between two bands at $E = 0$ or $E = \pm\pi$ (see Fig.S1(a)) and the maximal gap value around the same energies. From such maps we find that the full gap closing happens only at lines $\Theta_2 = 2\pi n$ with n being integer.

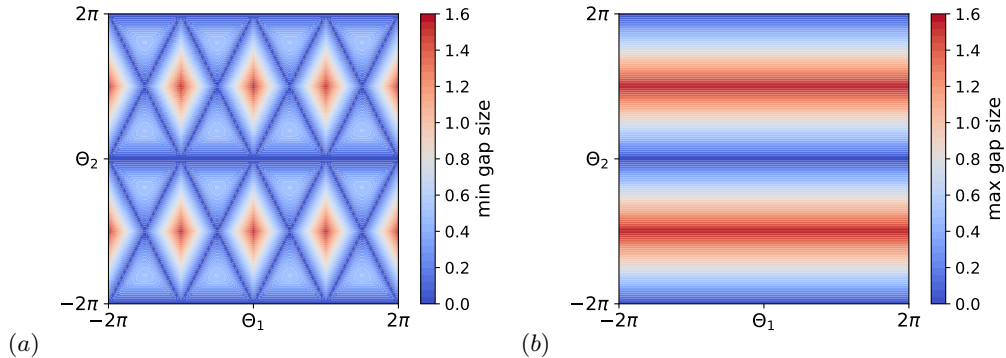


FIG. S1. The regions of one gap closing in panel (a) and both gaps closing in panel (b). Note the agreement between panel (a) and phase separation lines position.

The colormap of search dependence on defect parameters for the walker ‘1’ shown in Fig.2 of the main text is presented in Fig.S2. The dependence on Θ_2^{def} is absent, which motivates the studying of only different Θ_1^{def} values in the main text.

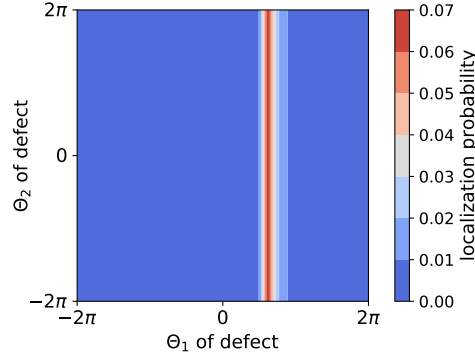


FIG. S2. @D colormap of dependence on defect parameters for a walker ‘1’. The optimal search is performed on a line - which demonstrates that the dependence on Θ_2^{def} is absent.

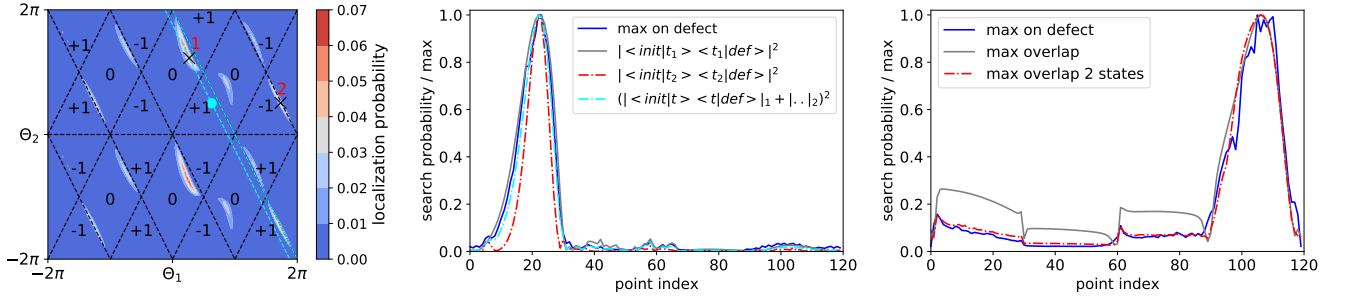


FIG. S3. Comparison of maximal product of overlaps described in the main text found over all eigenstates of evolution operator \bar{U} for a two lines in parameter space plotted as dashed cyan lines in the first panel. The second panel corresponds to a line going through walker ‘1’ and the third panel corresponds to a phase separation line.

The comparison of product of overlaps with optimal search regions

In this section we analyze how precise the correspondence between maximization of $|\langle d|n \rangle \langle n|i \rangle|^2$ and $(\sum_{n=\max_1, \max_2} |\langle d|n \rangle \langle n|i \rangle|)^2$ is compared to the regions of optimal search in parameter space for a fixed defect parameters. For this purpose we compare the max search probability curves plotted along two lines depicted as dashed cyan in the first panel of Fig.S3. One of these lines is a phase separation line and second one is parallel to phase separation and contains a walker ‘1’ discussed in the main text. This second line crosses different topological phases. In the second and third panels of Fig.S3 we plot the comparison of max probability found on time interval $T = 1000$ for the system size with $\sqrt{N} = 40$ with values of different overlaps. The second and third panels in Fig.S3 clearly demonstrate that the combination of maximum and second maximum products of overlaps - the contribution of two pairs of trapped states - describes the probability peak most precisely. This leads to a conclusion that efficient search is performed by two pairs of trapped states in this system in all cases studied.

Next, we analyze the structure of trapped states and their position in spectrum for the example walker parameters labeled as ‘2’. The analysis is similar to what is done in the main text and is presented in three panels of Fig.S4: comparison of search probability with overlap criteria in the first panel, the set of overlaps for each eigenstate of \bar{U} in second panel and the comparison of probability evolution at the defect with the one defined by the two pairs of the trapped states in the third panel. However, in this case we find that the two pairs of trapped states that mainly contribute to the efficient search are placed near zero energy. Also there is no gap in spectrum around this energy, but the in-gap trapped states placed around $E = \pm\pi$ do not contribute into the constructive interference relevant for successful search.

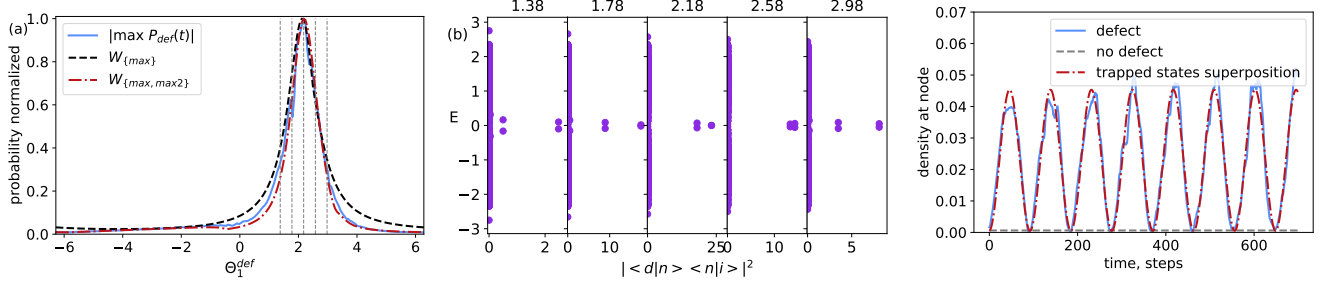


FIG. S4. (a) The comparison of search probability with overlap criteria for walker ‘2’. (b) The identification of states that mainly contribute into constructive superposition on a searched node for walker ‘2’ parameters. (c) The comparison of density evolution at searched defect node (blue solid line) with the superposition (red dashed line) of trapped states identified from panel (b).

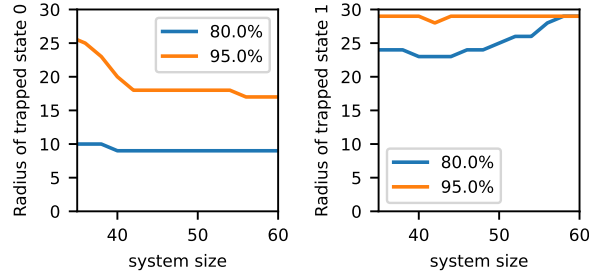


FIG. S5. Radius of trapped state as a function of system size. Left panel corresponds to a trapped state with largest overlap $|\langle d|n\rangle\langle n|i\rangle|$ in Fig.3(b) of the main text, and right panel corresponds to the state with second largest overlap.

Structure of trapped states in coordinate space

In this section we analyze how extended are the trapped states that mainly contribute to the search algorithm. From the search time dependence on system size shown in Fig.2(b) in the main text, we conclude that the more extended trapped state has radius $R \approx 50$ for walker ‘1’ and $R \approx 100$ for walker ‘2’ and defect parameter $\Theta_1^{def} = 5\pi/8$. The radius of trapped state was estimated as twice smaller than the system size where transition in time asymptotic happens. To further analyze the trapped state radius dependence on system size, we plot it in Fig.S5. The set of tested system sizes covers the region where the trapped states are having overlap with itself due to periodic boundary condition. To reduce the numerical precision issue related to identifying density of quickly decaying state far from its center, we plot a dependence of radius which covers 80% and 95% of density. Two plots show results for a state taken from each pair of trapped states discussed in the main text in Fig.3(b). The states from second pair have larger radius and it stronger depends on system size. Thus, the change in search time asymptotic is mostly defined by this second pair of trapped states, that has second maximal overlap value.

Stability of search algorithm with disorder

In this section we make a stability comparison of the proposed algorithm of search based on trapped states with Grover’s algorithm in split-step quantum random walk described in Ref.[7]. The size of the systems is taken to be the same - 512×512 nodes, well above the saturation time threshold for both example walker parameters described in the main text. Since the Grover’s algorithm relies on the coherent superposition of most states present in the system, one could expect that disorder break such constructive superposition faster than for a few trapped states. To check that, we implement the angle disorder of spin rotation matrices on each node. For equation (2) in the main text such disorder is introduced as

$$R(\Theta) \rightarrow R(\Theta + \delta\Theta_{xy}), \quad \delta\Theta \in [-\delta\Theta_{max}, \delta\Theta_{max}], \quad (S3)$$

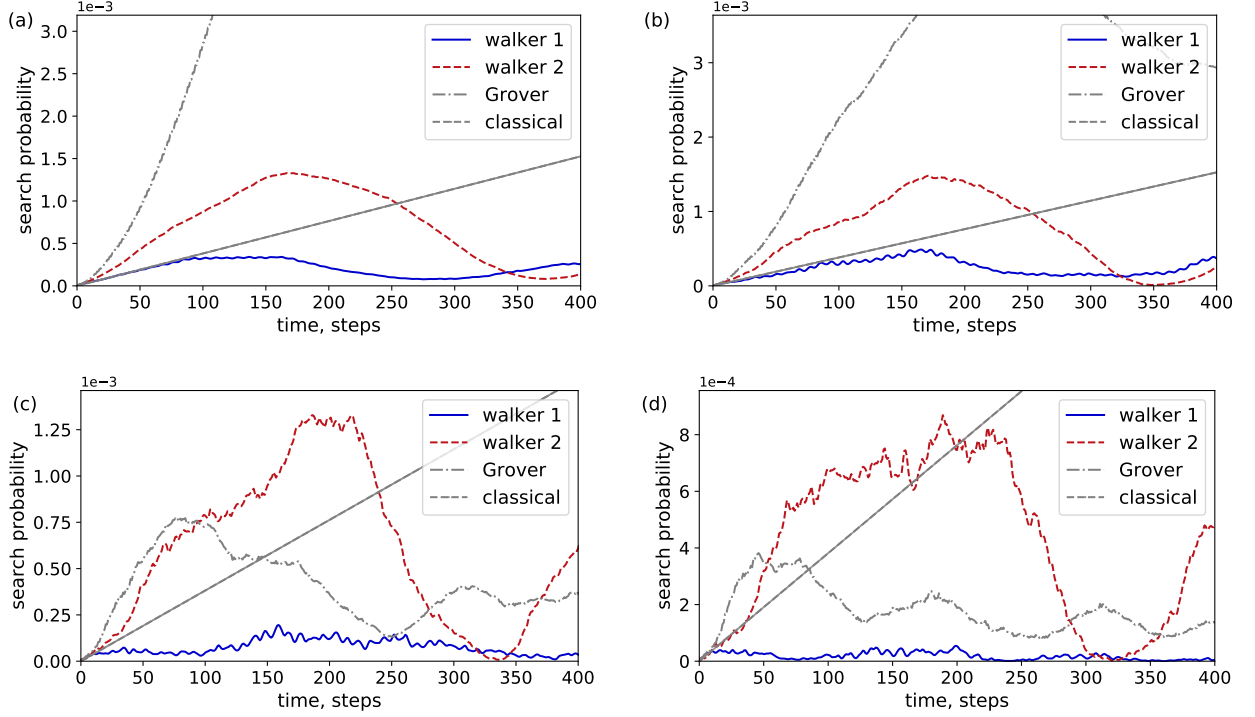


FIG. S6. The search probability calculated for 2 walker parameters analyzed in the main text (see Fig.2) and compared with Grover's algorithm in split-step QRW from Ref.[7] and with classical search with linearly increasing probability. The system size is 512×512 . Disorder strength varies from small in panel (a) $\delta\Theta_{max} = 0.05$, to (b) $\delta\Theta_{max} = 0.15$, (c) $\delta\Theta_{max} = 0.35$, and large in panel (d) $\delta\Theta_{max} = 0.5$. The walker 2 shows best performance at large disorder out of all compared search procedures.

where the distribution of $\delta\Theta_{xy}$ is uniform in the interval $[-\delta\Theta_{max}, \delta\Theta_{max}]$. Similarly, for the split-step QRW analyzed in Ref.[7] and used here as Grover's algorithm benchmark, the disorder is implemented as

$$C_x = \frac{1}{\sqrt{2}} \begin{pmatrix} 1 & i \\ i & 1 \end{pmatrix} \rightarrow C_x(\delta\Theta) = \frac{1}{\sqrt{2}} \begin{pmatrix} 1 & i \exp(i\delta\Theta) \\ i \exp(-i\delta\Theta) & 1 \end{pmatrix}, \quad (S4)$$

$$C_y = \frac{1}{\sqrt{2}} \begin{pmatrix} 1 & -i \\ -i & 1 \end{pmatrix} \rightarrow C_y(\delta\Theta) = \frac{1}{\sqrt{2}} \begin{pmatrix} 1 & -i \exp(i\delta\Theta) \\ -i \exp(-i\delta\Theta) & 1 \end{pmatrix}, \quad (S5)$$

The results of simulation for equal intervals of disorder angle are presented in Fig.S6.

The role of disorder in reducing efficiency of search algorithms is visible in all plots. However, for one of the two walkers, the search probability is always staying higher than the classical probability on the first period of oscillation. Notably, the probability of Grover's search drops dramatically. In the presented example of disorder configuration and type, the trapped state is demonstrating relatively stable behavior as a basis of search algorithm, even outperforming Grover's example for large disorder. Still, we point out that the more systematic study should be made to define the best performance conditions of different suboptimal quantum algorithms and compared with Grover's one in noisy quantum setups. Also one should note that these algorithms still outperform classical search, which behaves as $P_{classical}(t) = t/N$ with t being number of check ups of individual nodes.